Physica A 439 (2015) 7–19

Contents lists available at ScienceDirect

Physica A

journal homepage: www.elsevier.com/locate/physa

Motif-Synchronization: A new method for analysis of dynamic brain networks with EEG

R.S. Rosário [a], P.T. Cardoso [a], M.A. Muñoz [b], P. Montoya [c], J.G.V. Miranda [a,*]

[a] Institute of Physics, Universidade Federal da Bahia (UFBA), 40210-340 Salvador, Brazil
[b] Mind, Brain and Behavior Research Center (CIMCYC), University of Granada, 18010 Granada, Spain
[c] Research Institute on Health Sciences (IUNICS), University of the Balearic Islands, E-07122 Palma, Spain

HIGHLIGHTS

- We present a new method to evaluate synchronization between time series.
- Using time-varying graphs with synchronization methods, we evaluate EEG networks.
- Brain functional networks was able to differentiate affective processing in subjects.

ARTICLE INFO

Article history:
Received 11 February 2015
Received in revised form 11 July 2015
Available online 29 July 2015

Keywords:
Brain functional network
Motif-Synchronization
Time-varying graphs
EEG
Coupled Rössler oscillator
Chronic pain

ABSTRACT

The major aim of this work was to propose a new association method known as Motif-Synchronization. This method was developed to provide information about the synchronization degree and direction between two nodes of a network by counting the number of occurrences of some patterns between any two time series. The second objective of this work was to present a new methodology for the analysis of dynamic brain networks, by combining the Time-Varying Graph (TVG) method with a directional association method. We further applied the new algorithms to a set of human electroencephalogram (EEG) signals to perform a dynamic analysis of the brain functional networks (BFN).

1. Introduction

One of the major challenges of modern neuroscience is to understand how cognition emerges from the information flow within the brain. Functional brain connectivity, i.e. the measurement of the temporal and spatial synchronization among different brain regions, constitutes a helpful tool for this understanding. Functional brain connectivity is usually estimated from physiological signals, such as those obtained from the electroencephalogram (EEG) [1] or functional magnetic resonance imaging (fMRI) [2], by applying different methods derived from the theory of Complex Networks [3–5]. Accordingly, previous research has provided quantitative parameters by using Mutual Information [6], Pearson correlations [7], Granger Causality and spectral coherence [8] in order to analyze the preferred direction of the information flow between two adjacent nodes of brain networks during information processing or resting. However, these methods consider the brain as a static, rather than a dynamic complex network. Recently, it has been proposed that Time-Varying Graphs (TVG) may provide a unified framework for a detailed analysis of both static and dynamic characteristics of complex networks [9,10]. Thus, for instance, TVG formulations have been used to analyze the dynamic of functional neuronal networks from freely behaving rats [11] and functional connectivity from human EEG data [12].

* Corresponding author.
E-mail address: vivasm@gmail.com (J.G.V. Miranda).

http://dx.doi.org/10.1016/j.physa.2015.07.018
0378-4371/

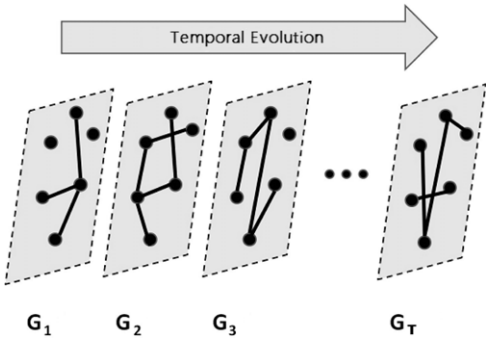

Fig. 1. Temporal evolution of the system with their graphs for each time t.

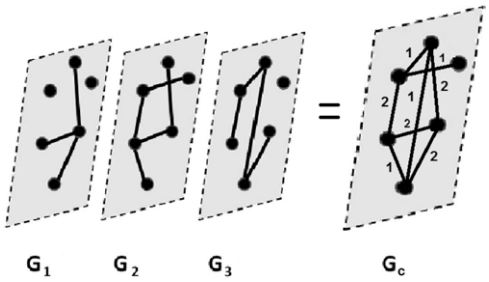

Fig. 2. Process of creating an ASN.

The major aim of the present work was to analyze the feasibility of a new method for the study of functional brain connectivity called Motif-Synchronization and based on TVG formalism. Motif-Synchronization provides the synchronization degree and direction between different nodes of a complex network by counting the number of occurrences of specific patterns within a time series. In the present study, we will analyze if this TVG method would be helpful to characterize the functional connectivity of a brain network generated from EEG data obtained in patients with chronic pain and healthy controls when performing a simple affective task.

2. Methods

2.1. Time-varying graphs

A time-varying graph can be described as an ordered sequence of graphs $G = \{G_t\}_{t=1,2,\ldots,T}$, where each G_t is a configuration of edges linking the vertices of the network at time t, and T is the total observation time of the system [9,10]. Fig. 1 shows a schematic example of a TVG.

2.2. Added static network (ASN)

Let $G = \{G_t\}_{t=1,2,\ldots,T}$ be a time-varying graph and $A_G = \{A_t\}_{t=1,2,\ldots,T}$ the set of the adjacency matrix of each graph G_t. The added static network (ASN) of G is given by:

$$A_c = \sum_{t=1}^{T} A_t. \tag{1}$$

The ASN is the sum of all adjacent matrices generated by the TVG method. Thus, A_c generates a weighted network in which the edges represent the dynamic property of the network over the time. Fig. 2 shows the process of creating an ASN.

2.3. Motif-synchronization (MS)

The waveforms of EEG signals can be described as a sequence of small patterns in a particular order of occurrence, which have been called Motifs [13,14]. Recently, several studies have proposed that these motifs can be used to build a method of association known as Permutation conditional mutual information [15–17]. Nevertheless, this method is too computationally expensive to be used within a TVG framework. In this paper, the motifs are used in a new simple way.

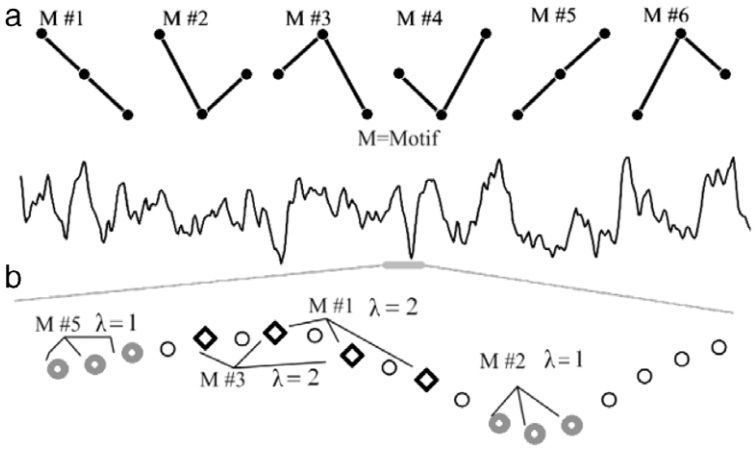

Fig. 3. (a) All motifs of degree for $n = 3$. (b) EEG signal and some possible motifs of degree $n = 3$ and lag $\lambda = 1$ (circle) or 2 (lozenge). *Source:* Modified from Ref. [17].

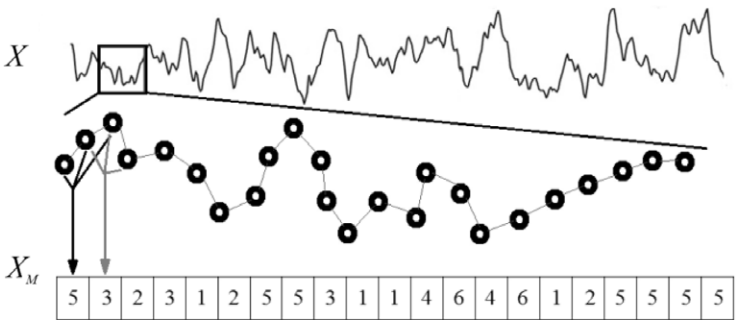

Fig. 4. Transformation of raw time series on motifs series.

The motifs can be usually classified as slopes, peaks or pits depending on the number of points used to generate each motif (motif degree) and the interval between these points (lag). The different motifs types can be automatically identified through a simple comparison between the values of the consecutive points of the time series. For example, for a degree $n = 3$ we have $n! = 3! = 6$ types of motifs. Fig. 3 shows some motifs with a degree value of 3 and different lags at $\lambda = 1$ and $\lambda = 2$.

Our method of Motif-Synchronization (MS) consists on counting the simultaneous appearance of these predefined patterns or motifs in two time series.

For a more detailed description of the method, let us assume two time series X and Y, which were simultaneously recorded. The first step of the method consists in the transformation of these time series into two new X_M and Y_M motifs series. For a degree $n = 3$, each element X_{Mi} can be defined as

$$X_{M_i} = \begin{cases} 1, & \text{if } X_i > X_{i+\lambda},\ X_{i+\lambda} > X_{i+2\lambda},\ X_i > X_{i+2\lambda} \\ 2, & \text{if } X_i > X_{i+\lambda},\ X_{i+\lambda} < X_{i+2\lambda},\ X_i > X_{i+2\lambda} \\ 3, & \text{if } X_i < X_{i+\lambda},\ X_{i+\lambda} > X_{i+2\lambda},\ X_i > X_{i+2\lambda} \\ 4, & \text{if } X_i > X_{i+\lambda},\ X_{i+\lambda} < X_{i+2\lambda},\ X_i < X_{i+2\lambda} \\ 5, & \text{if } X_i < X_{i+\lambda},\ X_{i+\lambda} < X_{i+2\lambda},\ X_i < X_{i+2\lambda} \\ 6, & \text{if } X_i < X_{i+\lambda},\ X_{i+\lambda} > X_{i+2\lambda},\ X_i < X_{i+2\lambda}. \end{cases}$$

Fig. 4 illustrates this procedure.

We define $c(X_M;\ Y_M)$ as the highest number of times in which the same motif can appear in Y_M shortly after it appeared in X_M for different delay times, i.e.,

$$c\,(X_M; Y_M) = c_{XY}$$

$$c_{XY} = \max\left(\sum_{i=1}^{L_m} J_i^{\tau_0}, \sum_{i=1}^{L_m} J_i^{\tau_1}, \ldots, \sum_{i=1}^{L_m} J_i^{\tau_n}\right), \tag{2}$$

with

$$J_i^{\tau} = \begin{cases} 1, & \text{if } X_{M_i} = Y_{M_{i+\tau}} \\ 0, & \text{else.} \end{cases} \tag{3}$$

The time delay τ range from $\tau_0 = 0$ to τ_n, where τ_n is the maximum value to be considered and L_m represents the size of a time-varying window within the time series. Similarly, we define the opposite measure c_{YX} by changing only the order of the time series in (3), $Y_{M_i} = X_{M_{i+\tau}}$.

The last step of the method is the definition of the degree of synchronization Q_{XY} and the synchronization direction q_{XY}, defined by

$$Q_{XY} = \frac{\max(c_{XY}, c_{YX})}{L_m} \tag{4}$$

and

$$q_{XY} = \begin{cases} 0, & \text{if } c_{XY} = c_{YX} \\ \text{signal}(c_{XY} - c_{YX}), & \text{else.} \end{cases} \tag{5}$$

The degree of synchronization is scaled between $0 \leq Q_{XY} \leq 1$, and q_{XY} will assume the value zero for a synchronization without preferred direction between X and Y, the positive value 1 when X precedes Y, and the negative value -1 when Y precedes X.

X. Li and G. Ouyang [17] proposed a method to obtain the optimal value of λ by using mutual information for two correlated time series. In our case, the use of this method to obtain the optimal value for each TVG edge would be extremely expensive in terms of computational time. In order to simplify and to increase the time resolution of our TVGs, we decided to use a constant value of $\lambda = 1$.

3. Applications

To study the feasibility of this new method, EEG data from five patients with chronic pain and five healthy controls were analyzed. Data were collected at the Research Institute on Health Sciences of the University of the Balearic Islands in Palma de Mallorca (Spain). Raw EEG signals were originally recorded from 31 channels, digitized at a sampling rate of 1000 Hz (resampled offline at 125 Hz) and filtered in the range of 0.1–70 Hz. Signals were acquired when participants were viewing a videoclip depicting a virtual walk through a park during 120 s under three experimental conditions: pleasant, neutral and unpleasant stimuli. The results of this study have been previously published elsewhere [18].

The first step was to generate a functional brain network, in which the EEG electrodes were considered the network nodes. In the present work, we used 31 EEG electrodes ($V = \{s1, s2, \ldots, s31\}$) placed according to the 10–20 International System. For each electrode, a time series of EEG data ($s_i(t),\ t \in [0; T]$, where T was the total time of the experiment) was obtained.

To analyze the functional connectivity of these networks, the Motif-Synchronization method was applied for the time series from each pair of nodes. The synchronization degree Q_{XY} in (4) and the synchronization direction q_{XY} in (5) were estimated for each edge (a_{ij}). The Q_{XY} of this network were statistically compared to a pre-set threshold value. This threshold value was obtained by shuffling all data points from each EEG time series, constructing a new random network, and selecting the value with a chance of 5% to be random in the network. If the Q_{XY} value for the edge a_{ij} was greater or equal than the threshold value, this edge was marked as $a_{ij} \equiv 1$, otherwise $a_{ij} \equiv 0$.

At the end of this process, the adjacent matrix of the network and the network indexes (weight degree and clustering coefficient) were obtained.

The process described above was performed for a given time window of size W. By computing the same parameters at different windows along the time series, time-varying networks were obtained. Fig. 5 illustrates the different steps of this procedure.

4. Results

Four different analysis of results are presented. In the first analysis, the ability of our MS method to detect driver response relationships was tested by using simulated data from unidirectionally coupled model systems. In the second analysis, the feasibility of our MS method to compute functional connectivity on real EEG data was compared with two other methods: Event-Synchronization [19] and Pearson correlation [11]. In the third analysis, the hub distribution of the functional networks was further examined by comparing EEG datasets from two subgroups of participants. In the last analysis, the global EEG network indices were compared in different experimental situations for two subgroups of participants.

4.1. Simulated data

In this section, we analyzed how the MS synchronization measures (Q_{XY} and q_{XY}) would respond to simulated data. We consider two coupled Rössler oscillator [20]:

$$\begin{aligned} \dot{x}_{1,2} &= -w_{1,2}y_{1,2} - z_{1,2} + \varepsilon_{2,1}(x_{2,1} - x_{1,2}), \\ \dot{y}_{1,2} &= w_{1,2}x_{1,2} + 0.165y_{1,2}, \\ \dot{z}_{1,2} &= 0.2 + z_{1,2}(x_{1,2} - 10), \end{aligned} \tag{6}$$

in order to analyze the detectability of the synchronization direction and degree of our proposed MS method.

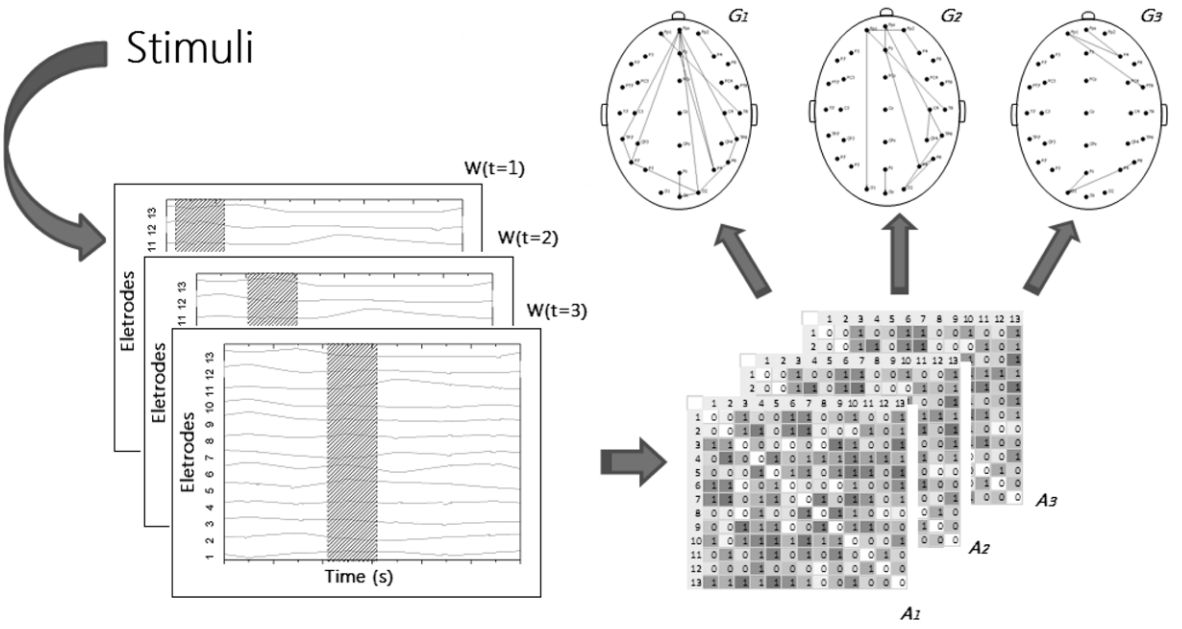

Fig. 5. Implementation of TVG method. For a given window of size W, a method of association was applied and a set of association matrices (weighted networks) was obtained. The gray scale of the matrices represents the magnitude of the association between the elements. A significance test was applied and the threshold value was obtained simplifying the association matrices to a set of adjacent matrices $\{A_i\}$. Each adjacent matrix represents a network in the TVG.

The equations of motion were integrated by using a fourth order Runge–Kutta algorithm with a step size of $dt = 0.1$. Twenty time series (2050 data points) were generated by using random initial conditions within a sphere with a radius of 0.5 centered at (1, 1, 1). The coupling strength ε_1 was varied between 0 and 1 in steps of 0.05 values ($\varepsilon_2 = 0$ since the second system was driven by the first one) and the natural frequencies of the oscillators were chosen as $w_1 = 0.89$ and $w_2 = 0.8$.

When the systems were uncoupled ($\varepsilon_1 = 0$), it is expected that our MS measures would have values around zero. By increasing the coupling strength, the measures should increase according with the growing influence of the driver system on the response system. The synchronization of the systems should lead to an adaptation of the response system to the dynamics of the controller. In this case, the detection of the driver's influence on the response system would be more difficult and may result in reduced values of the measures. In a completely synchronized state ($\varepsilon_1 = 1$), the dynamics of both systems will be identical [21]. The synchronization direction indices would be detected even for the highest values of coupling strength, since these types of coupled systems present synchronization with a phase delay. Fig. 6 shows the evaluated coupled system (Eq. (6)) with $\varepsilon_1 = 1$ and synchronization with a phase delay.

Fig. 7 shows the dependence of Q_{XY} and q_{XY} on ε_1 (for values between 0 and 1, in steps of 0.05).

As shown in Fig. 7, the MS method can correctly identify all indices of synchronization direction q_{XY} starting at a coupling strength of $\varepsilon_1 = 0.15$. We also noted that even for the highest values of the synchronization degree Q_{XY}, where it should be harder to detect the driver's influence on the response, the identification of indices of synchronization direction q_{XY} did not change. This result demonstrated the ability of the MS to detect the coupling direction, even for highly synchronized systems.

4.2. Comparison between methods

In this section, our MS method was computed on real EEG data and results were compared to those obtained from two already known methods for functional connectivity analyses: Event-Synchronization [19] and Pearson correlation [11].

The ASNs estimated with our MS method are displayed in Figs. 8 and 9 for two different subgroups of subjects (five patients with chronic pain and five healthy controls, respectively).

The weighted networks in Figs. 8 and 9 are quite different, probably due to the individuals variability.

The three methods for computing functional connectivity in EEG data were applied in two healthy controls (A2 and B2). For all three methods, the time window W had a fixed size of 200 ms, moving "point to point" in the time series for each TVG network.

For the MS method, we used a simplified version of the motifs with degree $n = 3$. This simplification considers motifs M#2 and M#4 the same, and motifs M#3 and M#6 the same (see Fig. 3). A lag $\lambda = 1$, and a delay time $\tau_n = 16$ ms were used. For the Event-Synchronization method [19], the events were defined as local maxima fulfilling the following additional conditions: (1) $X_i > X_{i+k}$, for $k = -K + 1, \ldots, 0, \ldots K - 1$; (2) $X_i > X_{i+k} + h$. We used $h = 0$, $K = 4$ points, and a fixed

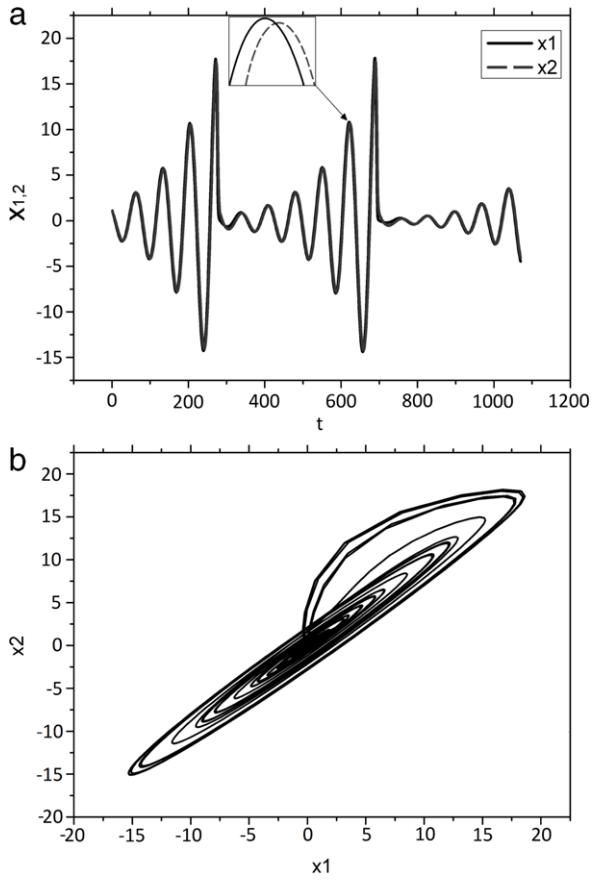

Fig. 6. (a) Coupled system from Eq. (6) with $\varepsilon_1 = 1,\ \varepsilon_2 = 0,\ w_1 = 0.89,\ w_2 = 0.8$ and synchronization with phase delay. (b) Lissajous curve showing the characteristic pattern of synchronized systems with phase delay.

maximum delay time of $\tau = 16$ ms. All parameters were determined so that the time window W was as small as possible, since a smaller window would hinder the definition of an effective amount of local maxima. For a very large window, the method would lose resolution for characterizing the dynamic activity of the brain.

To visualize topological similarities between networks obtained by each method, the ASNs were filtered by using those edges that appeared at least 10% of the time. Figs. 10 and 11 display the ASNs obtained from subjects A2 and B2, respectively.

Despite the differences on the number of edges obtained by each method, there were several nodes and edges that appeared as relevant for the three methods (represented as thicker edges in Figs. 10 and 11), especially when comparing the MS and the Pearson methods. Figs. 12 and 13 display pairwise scatter plots of edge values showing the similarities between the results obtained with the Motif-Synchronization and the two other methods in subjects A2 and B2, respectively.

All scatter plots displayed a segmented pattern with two correlation slopes and a threshold value around 1000 (as seen in Figs. 12 and 13). Table 1 shows the values of the determination coefficient obtained from pairwise correlations between the methods in all 10 subjects. These coefficients were calculated only for the range between 1000 and 10 000 of the edge's weights.

Most coefficients yielded significant values below 0.01, and only one coefficient was statistically non-significant.

In addition, the number of edges that were correctly detected in both the Motifs-Synchronization and the Event-Synchronization methods were counted. Table 2 shows the percentage of edges showing the same direction of synchronization when computed by these two methods in 10 individuals.

The average percentage of commonality in the previous analysis (Table 2) was 80.76%.

4.3. Hubs distribution

Hubs are defined as nodes with higher degree than the average degree of the network. In this work, hubs were defined as nodes where:

$$k_i(t) \geq \bar{k}(t) + 2\sigma(t) \tag{7}$$

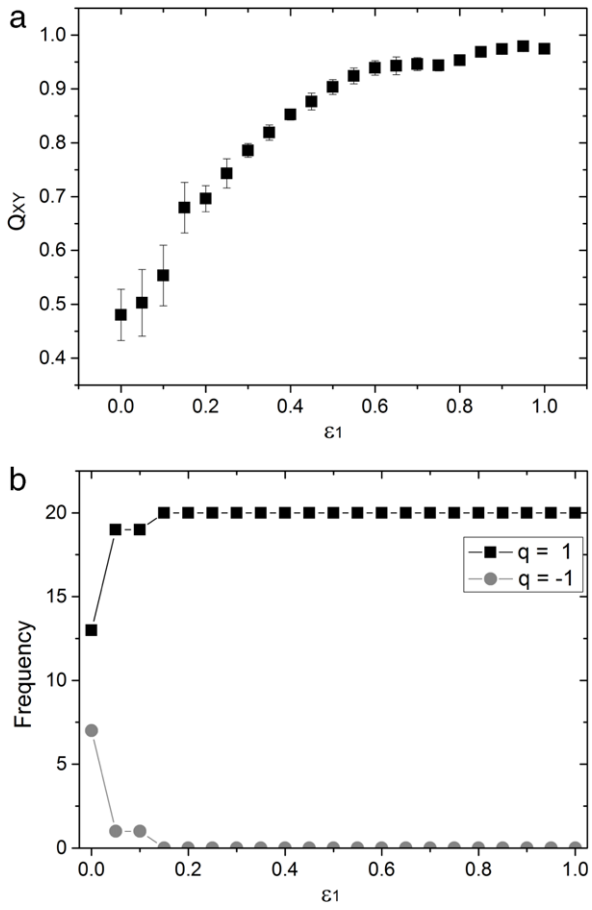

Fig. 7. (a) Influence of the coupling strength ε_1 on the synchronization degree Q_{XY} for coupled Rössler oscillators. (b) Influence of the ε_1 on the frequency of each q_{XY} values. System 2 was driving by system 1. Means, standard deviations and frequency obtained from 20 realizations of the x-components.

Table 1
Determination coefficients obtained from pairwise correlation between the methods.

Subjects	R^2 (ES × MS)	R^2 (PC × MS)
A1	0.378**	0.202**
B1	0.629**	0.675**
C1	0.188	0.365*
D1	0.569**	0.567**
E1	0.401**	0.359**
A2	0.807**	0.590**
B2	0.767**	0.878**
C2	0.606**	0.629**
D2	0.594**	0.263**
E2	0.417**	0.598**

* p-value < 0.05.
** p-value < 0.01.

where $k_i(t)$ was the degree of node i in time t, $\bar{k}(t)$ was the average degree, and $\sigma(t)$ was the standard deviation of all degrees within the network in time t.

In functional brain networks, hubs may represent brain regions with a highly relevant influence during cognitive processing. In directed networks, hubs may also represent two important features of brain activity: regions of concentration and diffusion. Concentration regions would be those receiving the highest flow of information during brain activation; whereas diffusion regions would be those sending the highest flow of information. Due to the dynamic feature of functional networks generated by our TVG method, it is possible to analyze the functioning and distribution of these hubs over the time. Figs. 14 and 15 show the distribution of hubs in subjects A2 and B2, respectively.

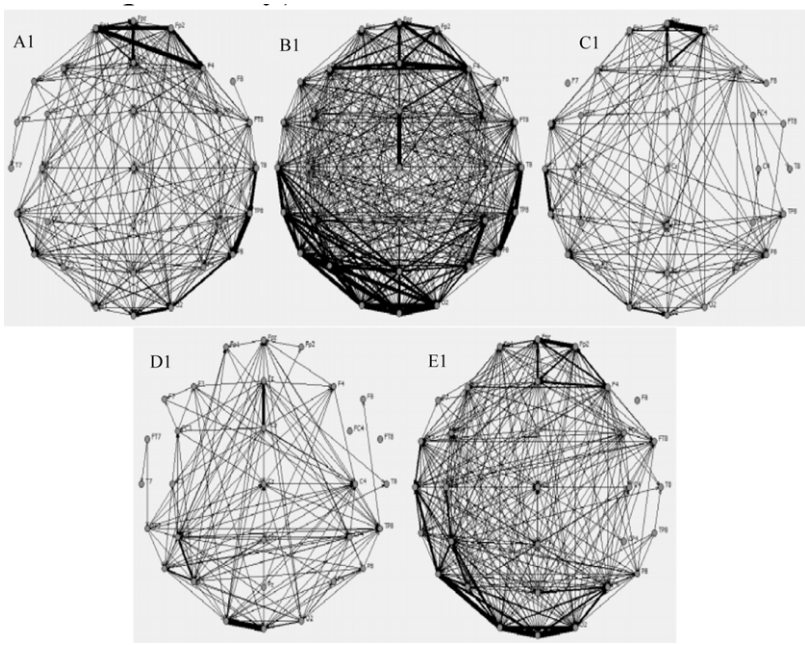

Fig. 8. Individual ASNs obtained with our MS method in a group of 5 patients with chronic pain. The thickness of the edges represents the strength of the association between two nodes of the network.

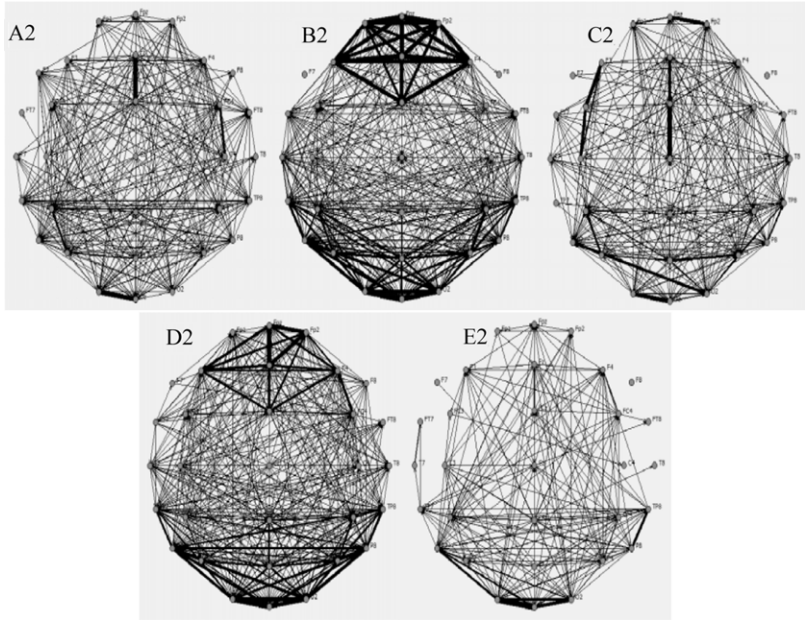

Fig. 9. Individual ASNs obtained with our MS method in a group of 5 healthy controls. The thickness of the edges represents the strength of the association between two nodes of the network.

Figs. 14 and 15 show that nodes located on frontal electrodes (Fp1, Fpz, Fp2, F7, F3, Fz, F4, F8, FT7, FC3, FCz, FC4, FT8) were considered more frequently output hubs than nodes located on occipital electrodes (O1, Oz, O2). By contrast, nodes located on occipital electrodes were considered more frequently as undirected or input hubs than nodes located on frontal electrodes. These results seem to indicate that frontal regions could act as a controlling brain area by sending information to other regions.

Finally, to test if there was some consistency in the distribution of these hubs across individuals, the probability distributions of the nodes were computed in 10 subjects. For this purpose, a cutoff value was defined as the mean plus

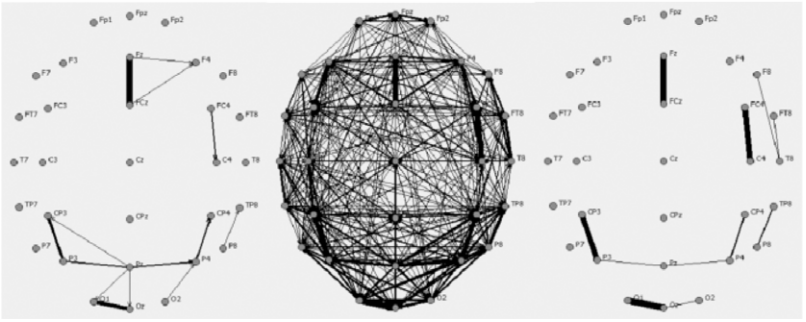

Fig. 10. ASNs obtained in subject A2 by Motif-Synchronization (left), Event-Synchronization (center) and Pearson correlation (right).

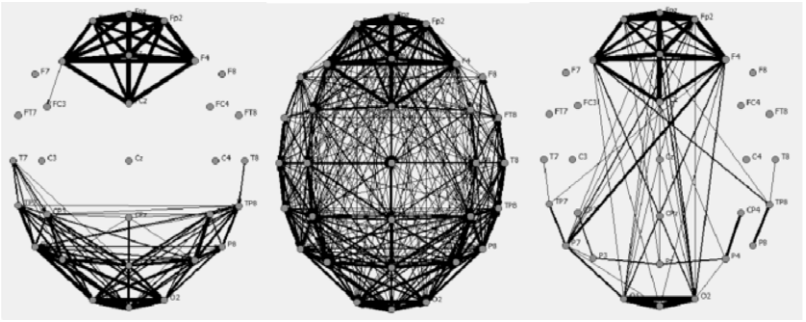

Fig. 11. ASNs obtained in subject B2 by Motif-Synchronization (left), Event-Synchronization (center) and Pearson correlation (right).

Table 2
Percentage of edges showing the same direction of synchronization when computed by the MS and the ES method.

Subjects	Percentage (%)
A1	70.37
B1	83.75
C1	80.3
D1	84.29
E1	71.38
A2	83.54
B2	82.68
C2	85.41
D2	80.66
E2	85.26

the standard deviation of the values for each hub. Fig. 16 shows the histograms for the most significant electrodes, with frequency indicating the number of individuals in which a specific node was higher than the cutoff value.

The histograms revealed that occipital (O1, Oz and O2) and Fz electrodes were representative of undirected hubs in several individuals, whereas Fz electrode was also representative of input and output hubs and FCz of output hubs. Taking into account that participants were involved in viewing a walk through a virtual park during EEG data acquisition, these findings may suggest that our MS method was able to identify the participation of brain regions relevant for information processing. In this sense, it should bear in mind that the occipital region is a primary projection brain area responsible for vision [22] and the frontal region is a secondary association area responsible for planning voluntary movements [22] and attention [23–25].

4.4. Comparing healthy controls and patients with chronic pain

The ASNs were also computed from EEG data collected in a group of 48 women (27 healthy and 21 patients with chronic pain) in two experimental conditions: looking at a fixation cross (BL), and viewing a videoclip inducing three different affective mood states: pleasant (PL), neutral (NT) and unpleasant (UN) [18]. From these EEG data, 192 ASNs were generated and the average weight degree was estimated for each ASNs. A Wilcoxon paired test was used to compare baseline ASNs with ASNs elicited by the three affective conditions. Fig. 17 shows the differences on the median weight degree between the baseline and the three affective conditions for both groups. These results demonstrated that our Motif-Synchronization

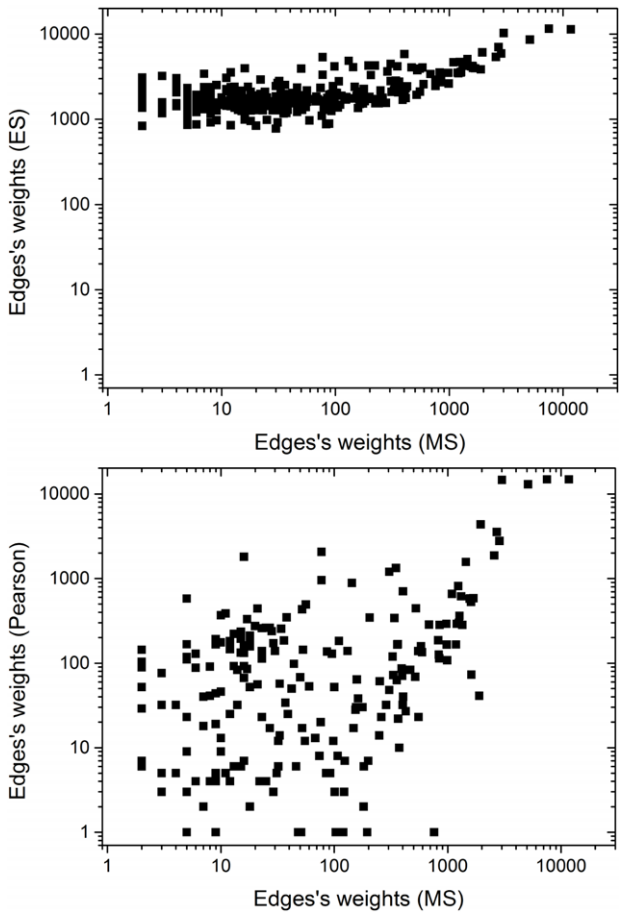

Fig. 12. Pairwise scatter plots of the edge weights as measured by the Motif-Synchronization and the Event-Synchronization (top) and the Pearson methods (bottom) in subject A2.

method was able to differentially discriminate between the functional brain networks elicited by different experimental conditions in healthy controls, but not in patients with chronic pain. In this sense, these results are in agreement with previous results obtained by using standardized measures of brain activity. Thus, for instance, previous work revealed higher EEG power (2–22 Hz) in response to the three affective conditions in patients with chronic pain, suggesting that these individuals might be characterized by an abnormal processing of affective information as compared to healthy controls [18].

5. Conclusion

This work proposes a new methodology for analyzing functional brain networks taking into account its dynamical properties. The new method is called Motifs-Synchronization (MS) and was compared with two other well-known methods for functional connectivity: Event-Synchronization and Pearson correlation. The application of the MS method to simulated data was able to correctly identify the coupling direction of two time series, even for highly synchronized systems. In the comparative analyses of different methods, we noted that results obtained from the application of our MS method to real EEG data were similar to those obtained with the two other methods.

Making a computational efficiency analysis of the methods, the PC method had the lowest average time of relative processing, about 8 s in the construction of each TVG. The ES method presented 10 s, while the MS method presented 20 s. Although the computational time of the Pearson correlation method is reduced, it does not provide an estimation of the direction of the synchronization and works only for no lag synchronous data. The computational time of the Event-Synchronization is also reduced and allows an estimation of the direction of the synchronization. Nevertheless, when this method is used with TVG, the minimal size of the TVG window is limited by the size of the event detection algorithm. By contrast, our MS method is fast and appropriate for TVG analysis, allows an estimation of the direction of the synchronization, takes into account different time lags and has no TVG window size limit. All these characteristics makes our method very feasible for dynamic analysis of brain networks.

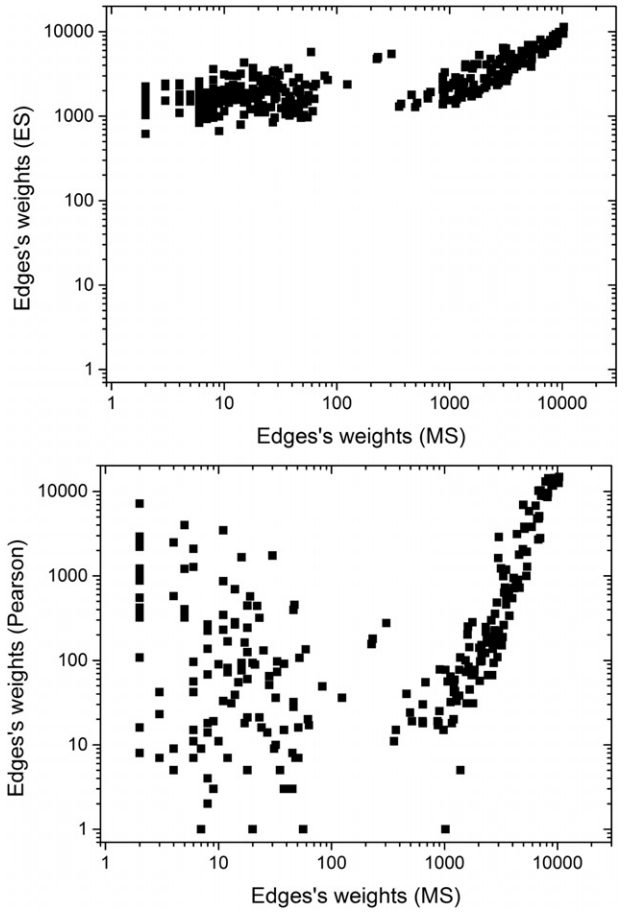

Fig. 13. Pairwise scatter plots of the edge weights as measured by the Motif-Synchronization and the Event-Synchronization (top) and the Pearson methods (bottom) in subject B2.

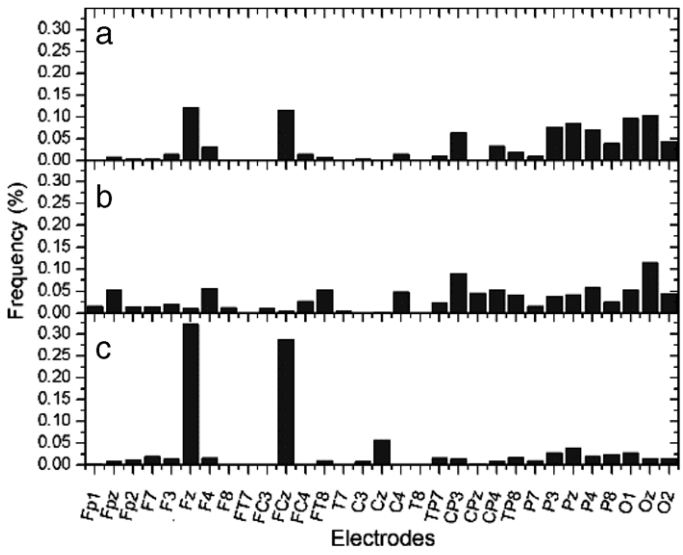

Fig. 14. Distribution of undirected (a), input (b) and output hubs (c) in subject A2.

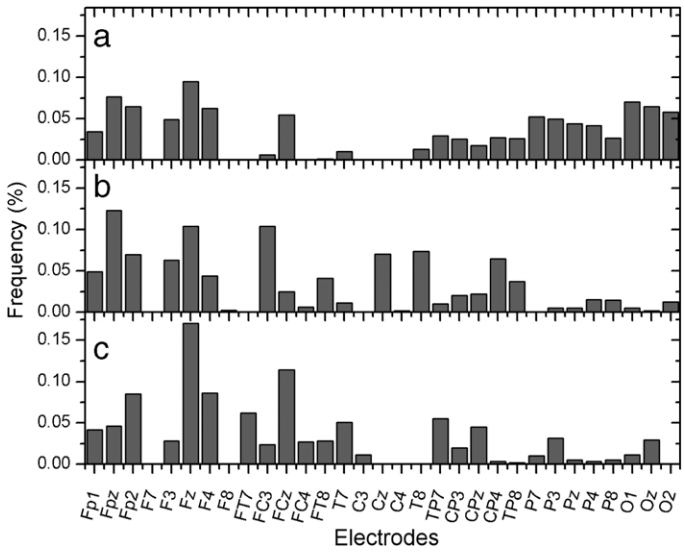

Fig. 15. Distribution of undirected (a), input (b) and output hubs (b) in subject B2.

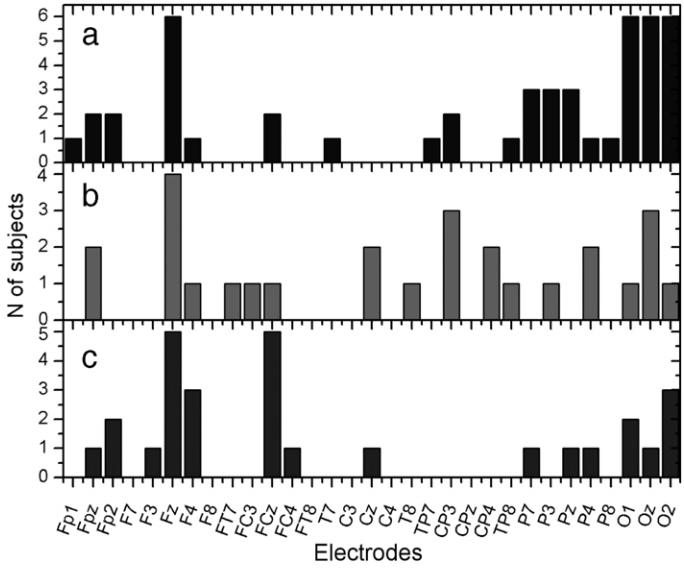

Fig. 16. Distribution of the most representative hubs: (a) undirected, (b) input and (c) output.

The analysis of hubs distribution and the ASN obtained with our MS method allowed the identification of relevant brain regions during information processing. We have observed that the most representative identified areas of the functional brain networks elicited during a visual processing task (viewing a walk through a virtual park) were located on frontal and occipital electrodes.

Finally, we demonstrated that our method was able to characterize the differences elicited by baseline and affective conditions on functional networks in patients with chronic pain and healthy controls. These findings are of special relevance since similar results have been found by using standardized methods for analyses of brain activity [18].

In conclusion, our findings revealed that Motif-Synchronization method could be a feasible tool for characterizing the dynamic evolution of functional brain networks [11,12,26]. Previous research on fMRI has already revealed relevant characteristics of the dynamic of these functional networks [27,28]. Nevertheless, the low temporal resolution of fMRI constitutes a serious limitation of this technique. The combined use of EEG, TVG, Added Static Networks [29] and the Motif-Synchronization, as it was proposed in the present work, constitutes a powerful tool for disentangling the complex dynamic of these functional brain networks.

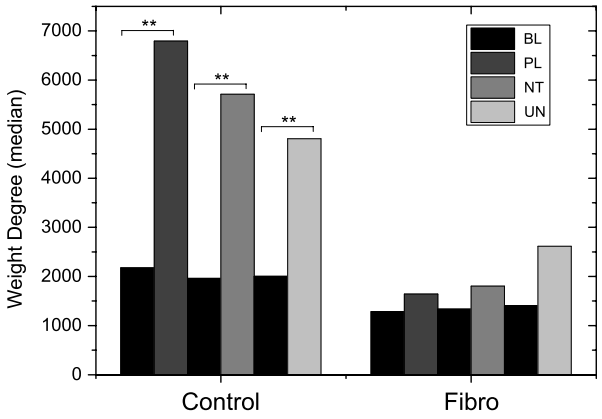

Fig. 17. Comparisons on the median weight degree of the ASNs elicited by baseline (BL), pleasant (PL), neutral (NT) and unpleasant (UN) conditions (** indicates p-values < 0.01 in the Wilcoxon paired tests).

Acknowledgments

The authors thank the Brazilian founding institution Fapesb for their financial support (#8778/2013). JGVM was supported by a Brazilian grant (CNPq, process 306571/2011-0). PM was supported by grants from the Spanish Secretary of State for R&D+i (#PSI2010-19372) and European Regional Development Funds (ERDF) (#PSI2013-48260).

References

[1] C.J. Stam, Int. J. Psychophysiology 77 (2010) 186.
[2] C.J. Stam, J.C. Reijneveld, Nonlinear Biomed. Phys. 1 (2007) 3.
[3] J.C. Reijneveld, S.C. Ponten, H.W. Berendse, C.J. Stam, Clin. Neurophysiol. 118 (2007) 2317.
[4] F.D.V. Fallani, et al., Nonlinear Biomed. Phys. 4 (2010) S8.
[5] F. De Vico Fallani, F.A. Rodrigues, L. Da Fontoura Costa, L. Astolfi, F. Cincotti, D. Mattia, S. Salinari, F. Babiloni, Brain Topogr. 23 (2011) 344.
[6] D. Meunier, R. Lambiotte, A. Fornito, K.D. Ersche, E.T. Bullmore, Front. Neuroinform. 3 (2009) 12.
[7] W. De Haan, Y. AL Pijnenburg, R.L. Strijers, Y. Van Der Made, W.M. Van Der Flier, P. Scheltens, C.J. Stam, BMC Neurosci. 10 (2009) 101.
[8] E. Bullmore, O. Sporns, Nat. Rev. Neurosci. 10 (2009) 186.
[9] J. Tang, S. Scellato, M. Musolesi, C. Mascolo, V. Latora, Phys. Rev. E 81 (2010) 055101.
[10] P. Basu, M.P. Johnson, R. Ramanathan, 1 (n.d.), 2010. Arxiv Preprint arXiv:1012.0260.
[11] B.B.M. Silva, J.G.V. Miranda, G. Corso, M. Copelli, N. Vasconcelos, S. Ribeiro, R.F.S. Andrade, Eur. Phys. J. B 85 (2012) 358.
[12] A.Y. Mutlu, E. Bernat, S. Aviyente, Comput. Math. Methods Med. 2012 (2012) 451516.
[13] C. Bandt, B. Pompe, Phys. Rev. Lett. 88 (2002) 174102.
[14] E. Olofsen, J.W. Sleigh, A. Dahan, Br. J. Anaesth. 101 (2008) 810.
[15] A. Bahraminasab, F. Ghasemi, A. Stefanovska, P. McClintock, H. Kantz, Phys. Rev. Lett. 100 (2008) 084101.
[16] Z. Li, G. Ouyang, D. Li, X. Li, Phys. Rev. E 84 (2011) 021929.
[17] X. Li, G. Ouyang, Neuroimage 52 (2010) 497.
[18] F. Rosselló, M.A. Muñoz, S. Duschek, P. Montoya, Psychosom. Med. (2015) in press, http://www.ncbi.nlm.nih.gov/pubmed/26186433.
[19] R. Quian Quiroga, T. Kreuz, P. Grassberger, Phys. Rev. E 66 (2002) 041904.
[20] O.E. Rössler, An equation for continuous chaos, Phys. Lett. A 57 (1976) 397.
[21] H. Osterhage, F. Mormann, T. Wagner, K. Lehnertz, Int. J. Neural Syst. 17 (2007) 139.
[22] A. Machado, Neuroanatomia Funcional, Atheneu, São Paulo, 2000.
[23] M.I. Posner, M.K. Rothbart, Annu. Rev. Psychol. 58 (2007) 1.
[24] M. Corbetta, Proc. Natl. Acad. Sci. USA 95 (1998) 831.
[25] R. Ptak, Neuroscientist 18 (2012) 502.
[26] D. Fraiman, G. Saunier, E.F. Martins, C.D. Vargas, PLoS One 9 (2014) e84612.
[27] R.P. Monti, P. Hellyer, D. Sharp, R. Leech, C. Anagnostopoulos, G. Montana, Neuroimage 103 (2014) 427.
[28] E.C.A. Hansen, D. Battaglia, A. Spiegler, G. Deco, V.K. Jirsa, Neuroimage 105 (2014) 525.
[29] V. Nicosia, J. Tang, M. Musolesi, G. Russo, C. Mascolo, et al., Components in time-varying graphs, Chaos 22 (2012) 023101.